JOURNAL OF Applied Polymer SCIENCE

Mechanical and UV-Shielding Properties of *In Situ* Synthesized Poly(acrylonitrile-butadiene-styrene)/Zinc Oxide Nanocomposites

Heriberto Rodríguez-Tobías, Graciela Morales, Oliverio Rodríguez-Fernández, Pablo Acuña

Departamento de Síntesis de Polímeros,, Centro de Investigación en Química Aplicada, Blvd. Enrique Reyna No. 140, (25253), Saltillo Coahuila, México

Correspondence to: G. Morales (E-mail: gmorales@ciqa.mx)

ABSTRACT: A series of poly(acrylonitrile-butadiene-styrene)/ZnO nanocomposites with different ZnO nanoparticles content were synthesized by a mass-suspension polymerization process. Nanocomposites obtained through this technique presented high impact resistance despite the presence of agglomerates for high ZnO nanoparticles content so that, these samples were subjected to twin-screw extrusion. The extrusion led to a dramatic morphological change and increased in impact resistance, higher than 100% in most of the cases. On the other hand, the higher the ZnO content, the higher the UV blocking (>95% for 1 and 3% of ZnO) for both materials, before and after extrusion. © 2012 Wiley Periodicals, Inc. J. Appl. Polym. Sci. 000: 000–000, 2012

KEYWORDS: ZnO nanoparticles; UV protection; poly(acrylonitrile-butadiene-styrene); mechanical properties

Received 22 March 2012; accepted 17 May 2012; published online
DOI: 10.1002/app.38092

INTRODUCTION

Outdoor applications of poly(acrylonitrile-butadiene-styrene) (ABS) are limited due to its vulnerability to ultraviolet radiation, which provokes rapid loss of impact strength (IS; main feature of this kind of materials) and yellowing[1–3] due to ABS chemical structure where the C-C double bonds can easily undergo photo-degradation. To mitigate this drawback several organic compounds, known as UV stabilizers, have been incorporated to ABS. Among these compounds are hindered phenols and amines, benzotriazole and benzophenone derivatives, organo-metallic compounds, etc.[4–6] Nevertheless, these organic UV stabilizers tend to migrate to the surface of the polymer item, are photo unstable and thermally unstable, and absorb in a narrow range of the ultraviolet spectrum[7–10] in spite of this, several of them must be used to have the desirable UV protection. Therefore, it is needed to find new alternative compounds that can act as UV stabilizer overcoming the shortcomings mentioned for the conventional ones.

Some recent reports demonstrate that the incorporation of zinc oxide nanoparticles (nano-ZnO) into different polymer matrices, such as poly(acrylonitrile),[11] poly(ethylene),[7] poly(propylene),[7,10] poly(styrene),[12] poly(methylmethacrylate),[9] and poly (ethylene terephthalate)[8] produces nanocomposites with excellent UV-shielding properties. Furthermore, the presence of nano-ZnO into a polymer matrix can affect positive or negatively on the thermal stability,[11–13] crystallization behavior,[8,11] and mechanical properties[7,10–12] of the obtained materials, which has been explained in terms of nano-ZnO dispersion, polymer-nanoparticle interactions, even to side reactions during nanocomposités synthesis.[13,14]

Nowadays there are few studies related to ABS/ZnO nanocomposites. Zhao et al.[15] investigated the influence of different amounts of nano-ZnO on the flammability and thermal properties of ABS/poly(ethylene terephthalate)/ammonium polyphosphate melt-mixed composites. It was determined that the polymer systems with 1–2% of nano-ZnO exhibited the best flame-retardancy rating (V0) during UL94 test and the limiting oxygen index was 29–30%. Furthermore, thermogravimetric analysis showed that the addition of nano-ZnO improved thermal stability and the yield of char residues of the studied systems. These facts were explained by possible reactions between the ammonium polyphosphate and the metal oxide nanoparticles. On the other hand, Díaz de León et al.[16] studied the mechanical properties of ABS/surface-modified ZnO nanocomposites synthesized by the *in situ* mass-suspension polymerization technique. The materials obtained showed an increase in IS of 29%, a slight decrease in the Youngs modulus and the rubber particlés morphology of the injection-molded products was rod like. However, these authors only analyzed the influence of one concentration of nano-ZnO and no further explanations are given neither in terms of the kinetics nor to the mechanical response.

This work deals with the effect of nano-ZnO content on mechanical and UV shielding properties of ABS-based

nanocomposites produced by *in situ* mass-suspension polymerization. Furthermore, the influence of twin-screw extrusion process on the above properties of the obtained materials was analyzed to provide theoretical basis for the ABS/ZnO nanocomposites preparation and processing.

EXPERIMENTAL

Materials

Styrene (St) from Plastiformas de México (Monterrey, México) and acrylonitrile (AN) from Sigma-Aldrich (St. Louis, Missouri) were used as received. The polybutadiene (PB) was supplied by Firestone (40% cis-1,4; 50% trans-1,4; and 10% vinyl units) (Lakes Charles, Louisiana). The aminosilane modified nano-ZnO of 13–28 nm in size were provided by Servicios Industriales Peñoles S.A. de C.V. (Torreón, México).

The initiators used were benzoyl peroxide (BPO) and tert-butyl perbenzoate (TBPB) from Promotores y Catalizadores Orgánicos de México. Tert-dodecyl mercaptane (TDM) (Sigma-Aldrich) was used as chain transfer agent. Polyvinyl alcohol (PVA), sodium chloride, and nonyl phenol were acquired from Sigma-Aldrich and used as received. Irganox 1076 (from Especialidades Químicas) and osmium tetra-oxide (Sigma-Aldrich) were used as thermal stabilizer and to stain samples for microscopic analysis, respectively.

The solvents used during the characterization of the obtained materials were acetone, methanol (industrial grade, from PROQUISA), and tetrahydrofuran (THF) (chromatographic grade, from Sigma-Aldrich). Finally, mineral oil (pharmaceutical grade) was used during reaction as viscosity reducer/controller.

Synthesis of ABS and ABS/ZnO Nanocomposites

Both, ABS and ABS/ZnO nanocomposites, were synthesized by the mass-suspension technique. First, PB (6 wt %), mineral oil (5 wt %), and a styrene/AN azeotropic mixture (77.4/22.6 wt %) were fed into a 1 gallon stainless steel reactor equipped with an anchor-turbine stirrer. The reactor was purged with nitrogen and the mixture was stirred at 30 rpm and at room temperature (approximately 15 h) to dissolve the rubber. Then 0.025 wt % of BPO, 0.2 wt % of TDM, and in the case of nanocomposites 0.05 to 3wt % of nano-ZnO were added to the reaction mixture, and the system was purged again, the stirring rate and temperature were increased to 60 rpm and 85°C, respectively and the stage of mass polymerization took place until the monomer conversion was close to 13–18%. During the mass stage, several samples were taken to determine the global conversion and Brookfield solution viscosity (10 wt % in toluene). The conversion was determined by dissolving 5 g of reaction mixture in 25 mL of toluene, followed by precipitation in 250 mL of methanol. The precipitated was dried to constant weight and the conversion was calculated. Thus, conversion is indicated as the ratio of the amount in grams of the precipitated sample to the amount in grams of the initial sample (both without the feed mass fraction of PB). Furthermore, some samples were subjected to mass polymerization without agitation (the results are not described herein). After the mass stage polymerization, the stirring was temporarily stopped; and 0.1 wt % of TBPB and the suspension medium were added to the reaction mixture. During this stage, the stirring rate was increased to 700 rpm and the temperature was kept at 125°C for 2 h and afterward at 150°C for 5 h. Subsequently, the obtained material (white beads) was washed and dried to constant weight at 70°C for approximately 24 h. The suspension medium was constituted by distilled water (2 L), PVA (3.5 g), sodium chloride (3.5 g), and nonyl phenol (0.9 g).

Molecular and Physicochemical Characterization

Gel content (GC) was determined by extraction, dissolving 0.25 g of the final product in 25 mL of acetone for 24 h at room temperature. Thereafter, the solution was subjected to 30 min of ultracentrifugation at 20,000 rpm and −20°C. The supernatant consisting of poly(styrene-*co*-acrylonitrile) (SAN) was precipitated from methanol, filtered and dried to constant weight. The insoluble was washed again with fresh acetone and the procedure described above was repeated for three times. Isolated SAN was redissolved in THF (high performance liquid chromatography grade) to evaluate the number-average molecular weight (M_n) by size exclusion chromatography. The weight percent of insoluble material and SAN copolymer were determined gravimetrically and through eq. (1) apparent grafting degree was estimated:

$$\mathrm{GD} = (\%\mathrm{gel\text{-}PB})/\mathrm{PB} \tag{1}$$

where, GD is the grafting degree, %gel is GC in percent, and PB is the initial fed rubber percentage.

IS Determination and Dynamic-Mechanical Analysis

Notched Izod IS test was carried out according to ASTM 256 at 25°C on compression-molded specimens, on a Custom Scientific Instrument 137 impact testing machine. Dynamic-mechanical analysis of specimens was performed on Q800 TA Instrument equipment, in cantilever bend mode at a frequency of 1 Hz and a deformation of 15 μm. The temperature range analyzed was from −120 to 120°C, the heating rate was 5°C/min.

Morphological and Elemental Analysis

Electron microscopic examination was carried out in a JEOL equipment in scanning-transmission mode (STEM), on samples cut (100 nm thickness) with a Leica Ultracut UCT ultra microtome and stained with osmium tetra oxide. Morphological parameters such as number–average rubber particle diameter (D_n), and the volume fraction of the rubber phase (Φ) were estimated from electronic micrographs with an Image J software through eqs. (2) and (3), respectively:

$$D_n = \mathrm{S}(L_i + H_i)/2n \tag{2}$$

$$\Phi = \sum A_i/A_t \tag{3}$$

where, L_i and H_i are the major and minor rubber particlés axis, respectively, n is the number of elastomeric particles counted, A_t and A_i are the total area of the micrograph and the area occupied by the rubber particles, respectively. Distribution and dispersion of nano-ZnO were determined by energy dispersive X-ray microanalysis in the aforementioned microscope in scanning mode (SEM).

Table I. Experimental Conditions and Maximum Conversion Achieved During the Mass Polymerization Stage for the Different ABS and ABS/nano-ZnO Composites Obtained

Reaction	Nano-ZnO[a] (wt %)	X_{max}[b]
A-0	0	13.88
A-0.05	0.05	15.28
A-0.17	0.166	16.07
A-1	1	18.28
A-3	3	13.97

[a]ZnO nanoparticles content, [b]Maximum conversion obtained during mass polymerization stage (160 min).

UV-Vis Spectroscopy of ABS and ABS/ZnO Nanocomposites Films

The UV-Vis spectra of compression-molded films (thickness of 250 ± 5 μm) of ABS and ABS/ZnO nanocomposites were determined using a UV-Vis spectrophotometer Varian Cary 500 in the wavelength range between 200 and 500 nm.

Extrusion of the Synthesized Materials

ABS or ABS/ZnO nanocomposites (mixed with 0.32 wt % of Irganox 1076) were extruded with a twin-screw extruder (diameter = 24 mm and length-diameter ratio = 40, Thermo Scientific Prism TSE 24MC) with screw rotating rate of 40 rpm, and the barrel settings temperature were: 200, 220, and 240°C. The extrudate was pelletized and dried at 70°C for 24 h. The impact resistance of the extruded samples was evaluated as previously described.

RESULTS AND DISCUSSION

Effect of Zno Nanoparticles on Kinetics and Phase Inversion

Table I condenses the experimental conditions and the maximum conversion achieved in the mass polymerization stage for the different nanocomposites obtained as well as the corresponding codes, where the number after the letter indicates the nano-ZnO content.

As the phase inversion (PI) is a crucial phenomenon that occurs during ABS mass-polymerization due to the rubber particles morphology establishment, the estimation of conversion range in which this phenomenon takes place was evaluated. In this sense, the evolution of conversion as a function of reaction time during the mass polymerization stage was first evaluated (Figure 1) for the ABS and ABS/ZnO nanocomposites. From Figure 1(a), it can be observed that the production of SAN copolymer slightly increases (respect to blank) with the increase of nano-ZnO content and it is more noticeable after 100 min of reaction. On the other hand, the M_n of the samples conducted to total monomer conversion decreases with ZnO concentration [Figure 1(b)]. These facts can be associated by one hand, to a possible catalytic effect of ZnO nanoparticles, as the C-C double bonds (both monomers) can be activated by the metal oxide surface leading to a Diels-Alder reaction between AN and styrene, and subsequently to auto-initiation of monomers (Scheme 1).[17] On the other hand, the decrease in M_n can be consider the result of transfer reactions between the groups located at the surface of the modified nanoparticles (amine moiety and hydroxyl groups) and the growing chains, according to literature (Scheme 2).[13,14,18] In turn, the radical formed on the α-methylene or hydroxyl group of aminosilane surface modifier can be deactivated by termination with a growing chain forming grafts onto the ZnO surface, as mentioned by Tsubokawa,[18] or by reaction between radicals and physisorbed water.[13,14]

These two events can affect the interval where the inversion phase takes place. To corroborate this assumption the reaction mixture's viscosity as a function of conversion was determined and plotted in Figure 2, where the PI can be detected by a decline in the viscosity curve followed by an increase in its

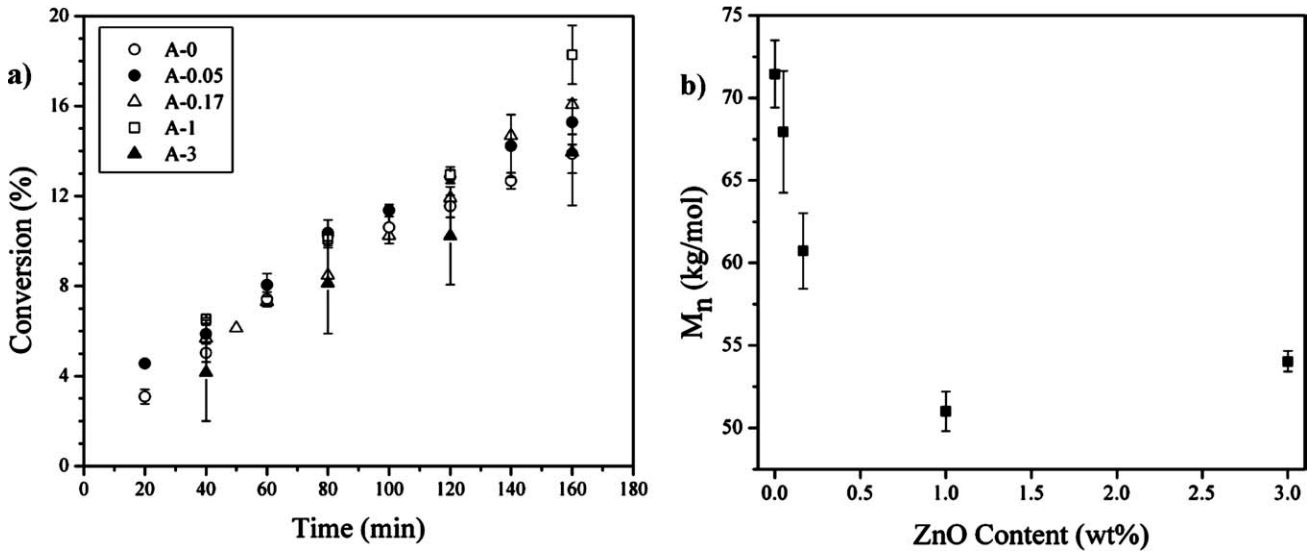

Figure 1. (a) Evolution of conversion during mass stage as a function of time and (b) Mn of the product obtained after 100% conversion as a function of nano-ZnO content.

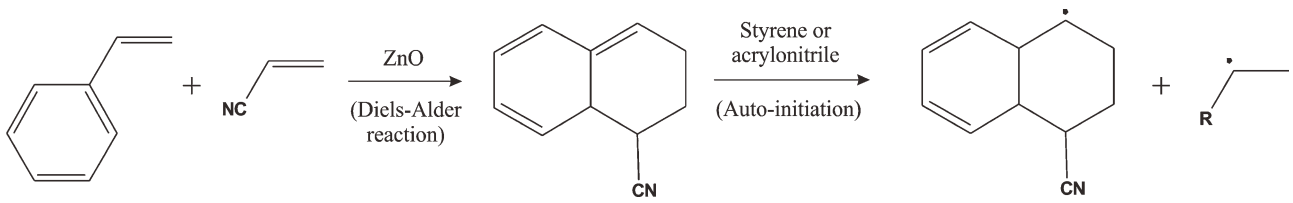

Scheme 1. Possible mechanism by which the nano-ZnO catalyzes Diels-Alder reaction and subsequently auto-initiation of the monomers.

values. In the case of A-0 (blank) and A-3 the PI takes place at conversion between 5–7% and 8–10%, respectively. In the other cases of A-0.05, 0.17, and A-1 it is difficult to establish by this technique the interval of conversion at which the PI occurs. However, the results suggest that PI was delayed in the presence of ZnO nanoparticles, which was corroborated by the micrographs shown in Figure 3, as A-0, A-0.05, and A-0.17 disclosed the typical salami rubber particles morphology at conversions of 7–8%, meanwhile, for A-1 and A-3 an interpenetrating network was disclosed for these conversion values, indicating an incomplete PI.

The delay in PI can be due to the difficulty of mass transfer,[19] as it was shown in Figure 2, the reaction mixture solutions in the presence of nanoparticles showed higher viscosity (up to 400%) in the conversion range analyzed. This fact can be explained in terms of chain polymer-nanoparticles interaction, as mentioned by Chae and Kim[20] in the case of polyacrylonitrile solutions. In the case of the particles used in this work, both ZnO surface and aminosilane modifier possess polar groups (hydroxyl and amino) which can form hydrogen bonds with the SAN matrix and/or SAN grafts.[21,22]

Morphology and IS of ABS Synthesized

In Figure 4 a series of micrographs corresponding to ABS and ABS/ZnO nanocomposites are shown. It can be observed that the presence of ZnO nanoparticles in the reaction medium did not affect the ABS morphology obtained, as all materials exhibited salami-type rubber particles, which is typical for ABS obtained by mass polymerization processes.[1,3]

Concerning to nanoparticles dispersion, ZnO agglomerates are not observed in specimens A-0.05 and A-0.17 by STEM technique. By contrast, in the case of A-1 and A-3 nanocomposites, ZnO is not uniformly dispersed. This fact can be explained in terms of ZnO nanoparticles interactions, which increase with higher content and consequently form agglomerates.[23] Furthermore, to contrast metal oxide and organic (SAN and PB) phases of ABS nanocomposites with lower nano-ZnO content, it was carried out the elemental mapping of zinc, and the micrographs are shown in Figure 5. By this technique, it was confirmed that at low contents of nano-ZnO a good dispersion is achieved. Moreover, in the case of A-3 sample [Figure 5(c)] instead of the presence of some agglomerates, a large proportion of nanoparticles are well dispersed in the polymer matrix.

With respect to the mechanical properties of ABS, it is well-know that the IS depends on several morphological and molecular parameters of both SAN matrix and rubber phase.[2,3] Besides, the dispersion of nanoparticles is another important factor that affects impact performance of nanocomposites.[24–26] Table II shows the Izod IS for the obtained materials. First of all, it can be observed that ABS with the lowest ZnO content exhibits the major IS and then this property has a slight decrease with increasing ZnO content. Taking into account the determined molecular parameters it is possible that this behavior can be associated to the fact that in the case of A-0.05, the

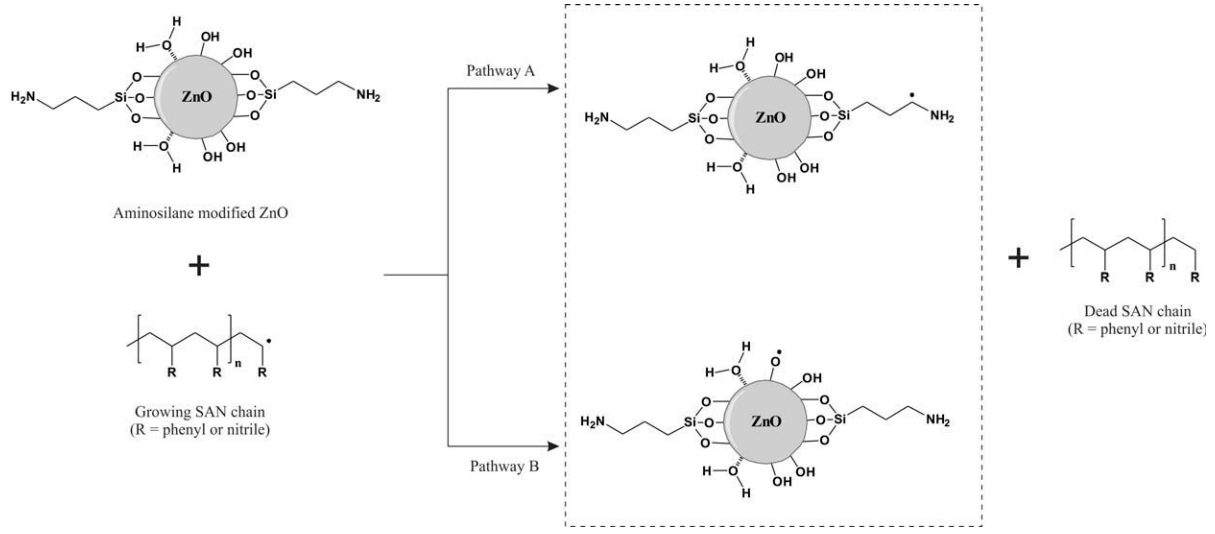

Scheme 2. Transfer reaction between growing SAN chains and aminosilane modifier (Pathway A) and/or hydroxyl groups (Pathway B) onto ZnO surface.

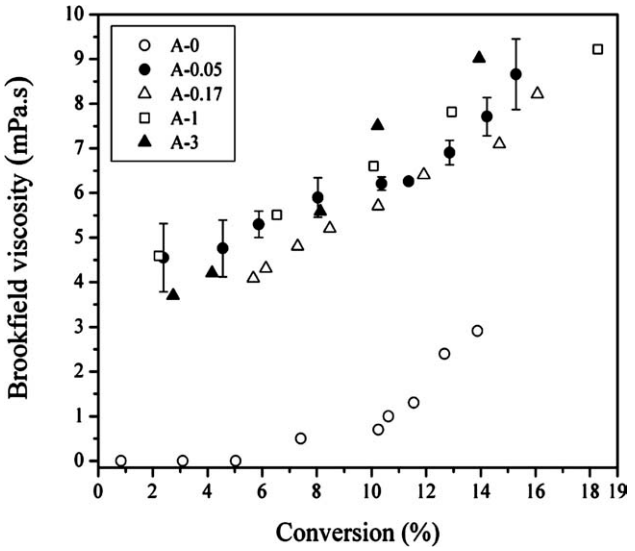

Figure 2. Reaction mixture viscosity as a function of conversion during ABS and ABS/ZnO nanocomposites synthesis.

values of Φ and GC are higher than that corresponding to A-0 (blank) and to an optimal D_n (see Table II). Furthermore, the presence of well-dispersed nanoparticles makes plastic deformation easier (i.e., higher energy dissipation).[24–26] On the other hand, when ZnO content is higher than 0.05% and as morphological parameters are practically the same as A-0.05, the slight drop in impact values can be attributed to the existence of agglomerates (approximately from 3 to 5μm in size) in the ABS matrix, which can act as stress concentrator sources that lead to a rapid fracture growth.[24–26] It is important to mention that although matrix molecular weight exhibits variations as a function of ZnO content, the effect on mechanical performance can be discarded as it is reported in literature that matrix average-number molecular weight greater than 60 kg/mol have no effect on the IS.[3]

Dynamic-Mechanical Analysis of ABS and ABS/ZnO Nanocomposites

Due to its heterogeneous nature, ABS shows a characteristic dynamic mechanical behavior, which is disclosed in Figure 6. Both peaks at low and high temperature can be considered as

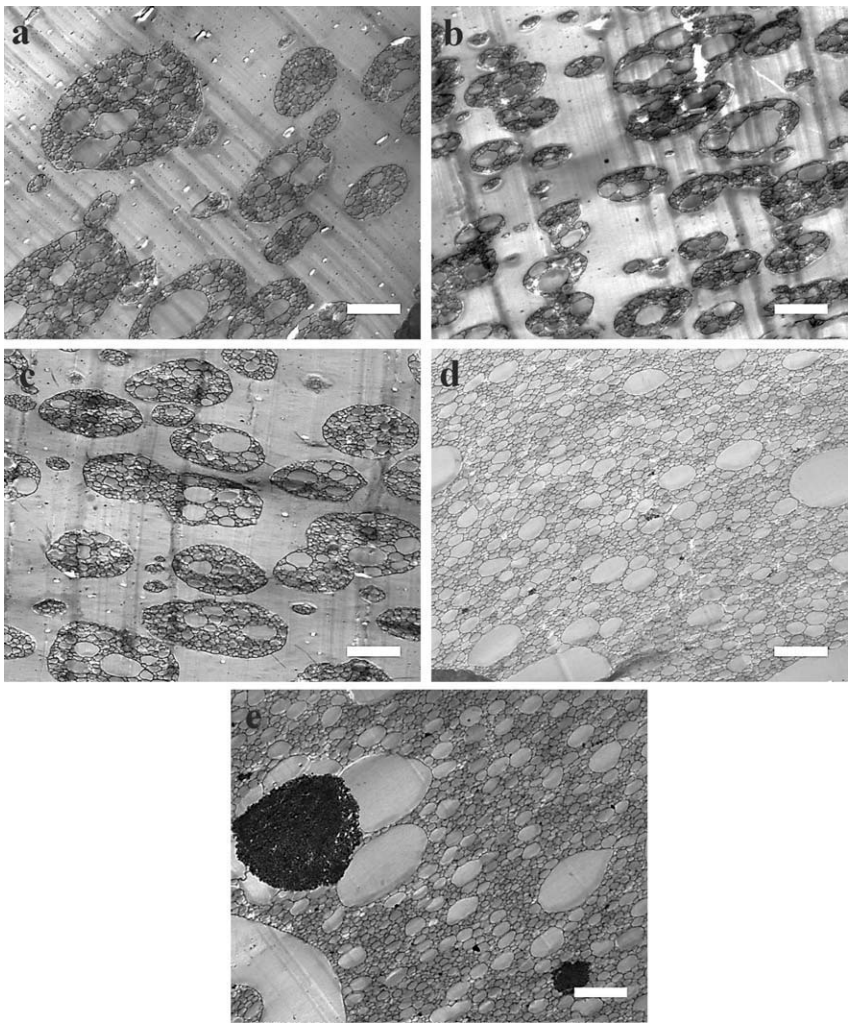

Figure 3. ABS and ABS nanocomposites morphology obtained at different conversion values during the mass polymerization stage. (a) A-0 at 7.4%, (b) A-0.05 at 8%, (c) A-0.17 at 8.4%, (d) A-1 at 10.1%, and (e) A-3 at 8.3%.

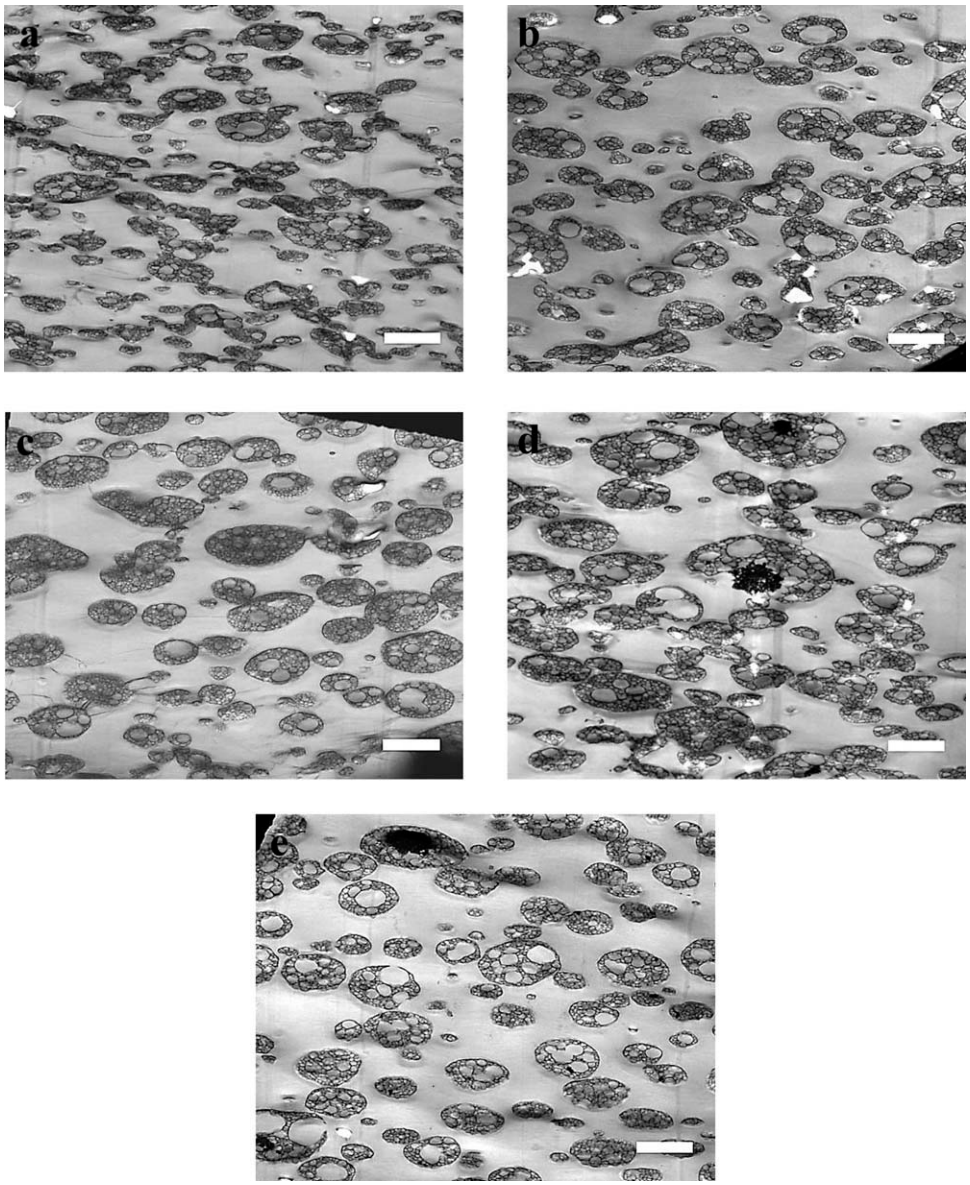

Figure 4. Scanning-transmission electronic micrographs for (a) A-0, (b) A-0.05, (c) A-0.17, (d) A-1, (e) A-3 (scale bar = 3 μm).

the corresponding glass transition temperatures (T_g), T_g of PB phase at low temperature and T_g of the SAN matrix at high temperature. Even though these two peaks are present in all the synthesized materials, in the presence of nano-ZnO, a peak displacement to high temperature (high T_g values) of both, dispersed and continuous phase, occurs (see Figure 7), and this displacement is more evident with high nanoparticles content. As morphological parameters do not exhibit substantial changes, the increase in T_g can be explained by two theories: (i) possibly ZnO-polymer chain (PB, SAN matrix, and/or grafted SAN) interaction as previously mentioned, that leads to a restriction of macromolecular chain movements and/or (ii) macromolecular confinement, as during *in situ* polymerization polymer chains can be trapped between nanoparticles. In fact, in the studied systems the higher the ZnO content, the higher the T_g[23,20].

UV-Shielding Properties of the ABS and Respective Nanocomposites

To investigate the effect of the incorporation of different nano-ZnO content on the UV-shielding properties of the synthesized materials, UV transmittance spectra of nanocomposites and pure ABS were determined and plotted in Figure 8. By this spectroscopic technique, the inherent UV absorption of pure ABS can be corroborated. On the other hand, the nanocomposites containing a low nano-ZnO content (A-0.05 and A-0.17) exhibits minor transmittance than the blank, this indicates that ZnO nanoparticles block and/or absorb UV rays. Moreover, the increase of nanoparticles content in the nanocomposites reduces remarkably the transmittance especially from 300 to 380 nm (UVA) and reaches a minimum value for 1%. Interestingly, the transmittance of A-3 is higher than A-1 (i.e., lower UV-shielding), which can be attributed to the agglomeration of nano-

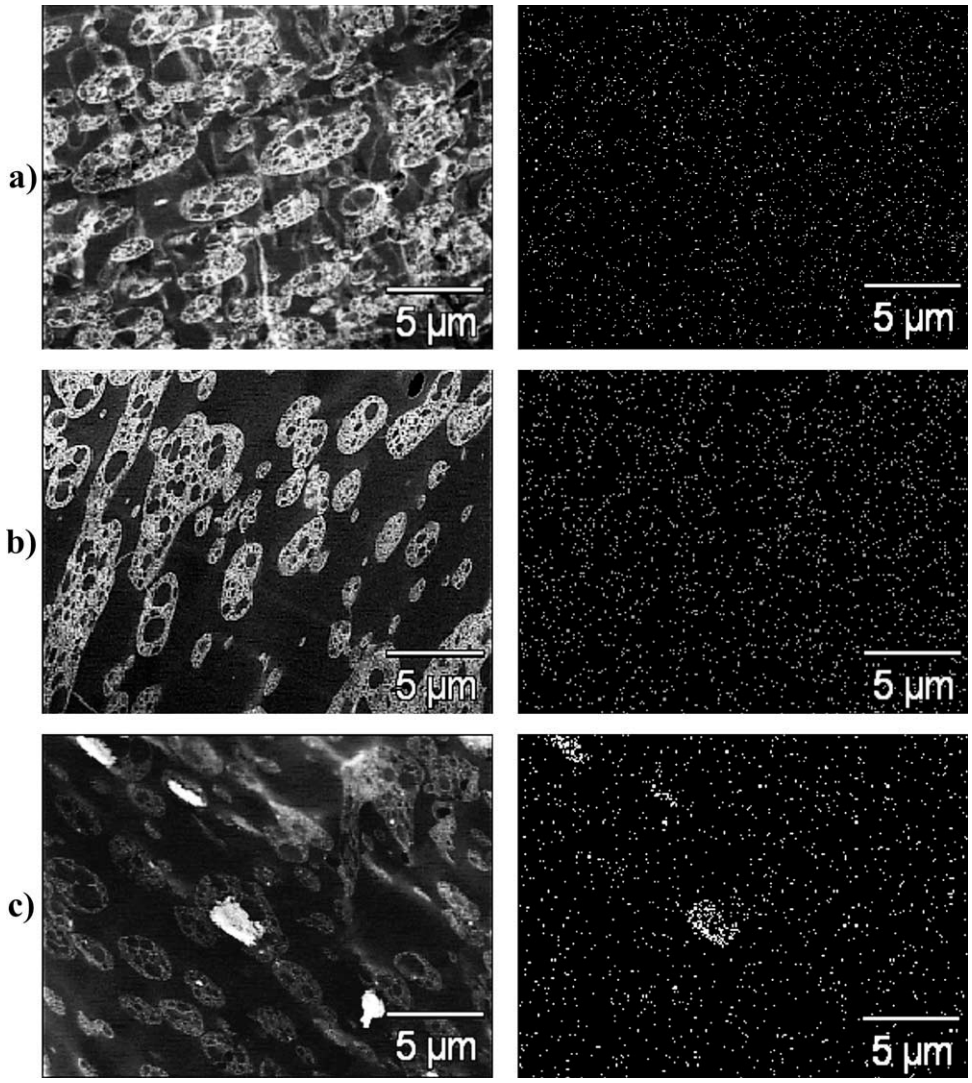

Figure 5. Micrographs of the obtained ABS/ZnO nanocomposites: (a) A-0.05, (b) A-0.17 and (c) A-3 (left: scanning electron, right: elemental mapping by EDX where white dots represent location of zinc element).

ZnO, that leads to a decrease of surface area prone to protect against UV radiation. Based on the exposed results, it can be established that ZnO nanoparticles are potential inorganic UV shield for ABS, mainly in the UVA range.

Effect of Twin-Screw Extrusion Process on ABS and ABS/ZnO Nanocomposites Properties

Due to the presence of some agglomerates into ABS nanocomposites, these materials were passed throught a twin-screw

Table II. Morphological, Molecular, and Compositional Parameters for ABS and ABS/ZnO Nanocomposites

ABS	IS (J/m)[a]	M_n (kg/mol)[b]	D_n (mm)[c]	Φ[d]	Gel (%)[e]	GD[f]
A-0	96.81	77.96	1.25	0.308	14.62	143.67
A-0.05	108.24	96.83	1.49	0.366	16.30	171.67
A-0.17	92.22	86.50	1.66	0.305	ND	ND
A-1	90.43	76.02	1.56	0.346	19.70	228.33
A-3	86.31	80.03	1.55	0.387	14.88	148.00

[a]IS, Izod impact strength, [b]M_n, number-average molecular weight determined by SEC, [c]D_n, number-average rubber particle diameter obtained by STEM micrographs, [d]Φ, rubber phase volume fraction determined from STEM micrographs and through eq. (3), [e]Gel, gel content gravimetrically determined, [f]GD, apparent grafting degree obtained through eq. (1).
ND: not determined because no phase separation was achieved by dispersion-centrifugation technique.

Applied Polymer SCIENCE

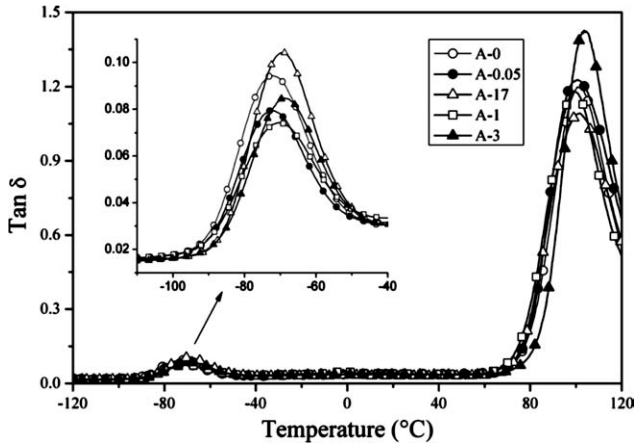

Figure 6. Tan δ as a function of temperature of ABS and ABS/ZnO nanocomposites.

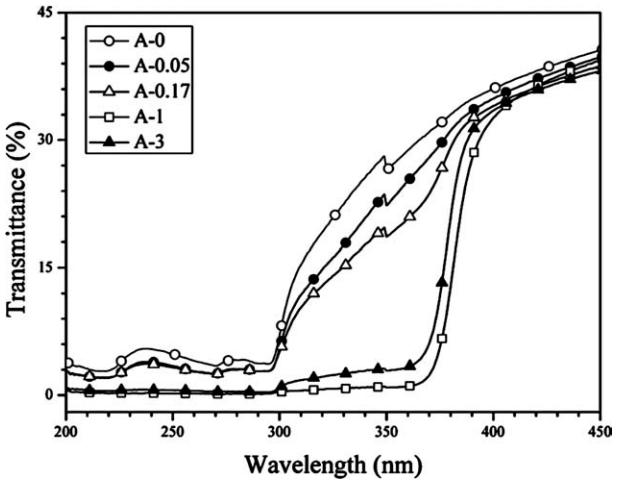

Figure 8. Transmittance UV-Vis spectra of ABS and ABS/ZnO nanocomposites films.

extruder. In Figure 9, the morphologies of the extruded ABS and ABS/ZnO nanocomposites are shown. It can be clearly observed the reduction in the agglomerates size (<2 μm). However, the salami rubber particles of all these materials were fragmented by the extrusion process, which resulted in a decrease in Φ in the order of 50% (see Table III), as occluded SAN migrates to the continuous SAN phase. The fragmentation of the rubber particles may be due to an excessive shear stress generated inside the twin-screw extruder and/or to the absence of sufficient crosslinking in the rubber phase as the maximun conversion value reached was in the order of 90%. On the other hand, GD values of all the materials increased when they were subjected to the extrusion process, which can be atributted, as mentioned by Soriano et al.,[27] to grafting reactions during processing.

In a similar way that it was mentioned before, the dispersion of nano-ZnO is difficult to determine due to the low contrast of phases, specially between ZnO and PB, to overcome this problem the elemental mapping technique was used and the corresponding micrographs are shown in Figure 10. It can be seen that all the ABS nanocomposites exhibit highly homogeneous dispersion of nano-ZnO, although STEM derived images show some agglomerates.

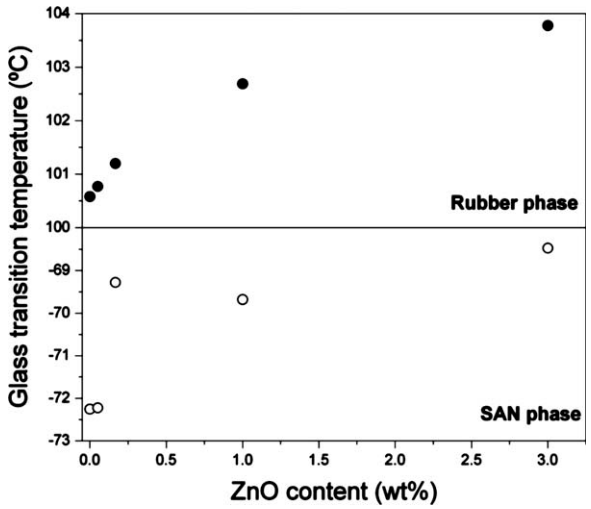

Figure 7. Glass transition temperature (T_g, corresponding to maximum Tan δ value measured by DMA) for the rubber and SAN phases as a function of nano-ZnO content.

Regarding to the impact properties of the extruded ABS nanocomposites, despite the morphological change of the elastomeric phase mentioned above, Izod impact values were doubled compared with the respective materials before extrusion process (see Figure 11). Moreover, impact behavior of extruded materials has the same behavior compared with materials before extrusion, that is, maximum Izod impact occurs with 0.05 wt % of nano-ZnO, and as the ZnO nanoparticles content increases the IS values decrease. The improvement in impact properties of the extruded materials can be attributed to three factors: (i) the morphological similarity between rubber particles of these materials and commercial ABS obtained by emulsion polymerization technique, which possesses greater impact resistance,[2,3] (ii) higher GD values which promote better stress transfer between SAN matrix and elastomeric particles,[28] and (iii) a better dispersion and/or size decrease of the nano-ZnO agglomerates.[24–26]

In relation to the UV properties of the extruded materials, Figure 12 shows the UV-Vis spectra of the extruded ABS and the respective nanocomposites. Practically, transmittance behavior follows the same pattern than those of the materials before the extrusion process, that is, the higher the nano-ZnO content, the higher UV-shielding (lower transmittance). The anomalous behavior previously observed in the analysis of UV transmission spectroscopy for high ZnO concentration was overcome and now it follows a normal tendency as it directly depends on ZnO content.

Interestingly, there was a decrease in transmittance (increase of UV protection) for the ABS without nanoparticles, which may be due to an increase in the surface area, as when rubber particles were fragmented by extrusion, the surface area was increased and therefore, the exposition to UV radiation was major.

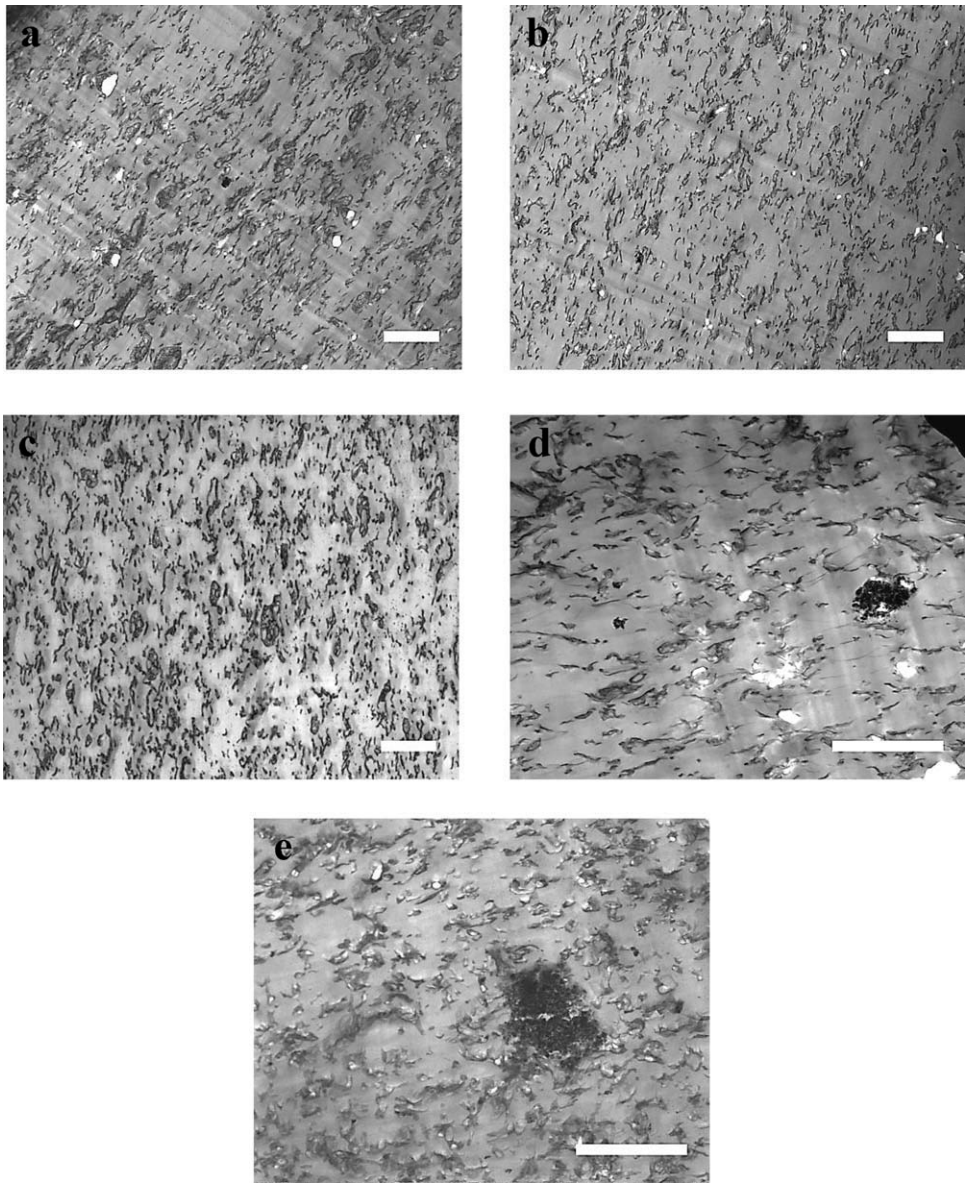

Figure 9. Scanning-trasmission electronic micrographs of extruded materials. (a) A-0, (b) A-0.05, (c) A-0.17, (d) A-1, and (e) A-3 (scale bar = 3 μm).

Table III. Morphological, Molecular, and Compositional Parameters of ABS and ABS/ZnO Nanocomposites after Extrusion

ABS	M_n (kg/mol)[a]	Φ[b]	Gel (%)[c]	GD[d]
AE-0	66.87	0.230	19.45	224.17
AE-0.05	72.76	0.166	20.41	240.17
AE-0.17	64.84	0.200	18.89	214.84
AE-1	72.42	0.168	21.26	254.38
AE-3	68.75	0.246	16.73	178.89

[a]M_n, number-average molecular weight determined by SEC, [b]Φ, rubber phase volume fraction determined from STEM micrographs and through eq.(3), [c]Gel, gel content gravimetrically determined, [d]GD, apparent grafting degree obtained through eq. (1).

CONCLUSIONS

The synthesis of ABS and/or nanocomposites based on ABS/nano-ZnO through the bulk-suspension processes give rise to salami type morphologies and the nano-ZnO are preferably located at the rubber phase as agglomerates. The nanocomposites obtained through bulk-suspension process present a better IS in comparison with the reference ABS, the IS increased 11% at 0.05% of ZnO. As nano-ZnO content increases, the IS decreases due to the presence of ZnO agglomerates.

In the ABS obtained after extrusion, the IS doubles the values obtained before extrusion due to morphological changes and a better dispersion of the nanoparticles into the matrix.

The dynamic mechanical analysis of synthesized materials showed an increase of T_g for both rubber and matrix phases in the presence of nano-ZnO, which can be due to

Applied Polymer SCIENCE

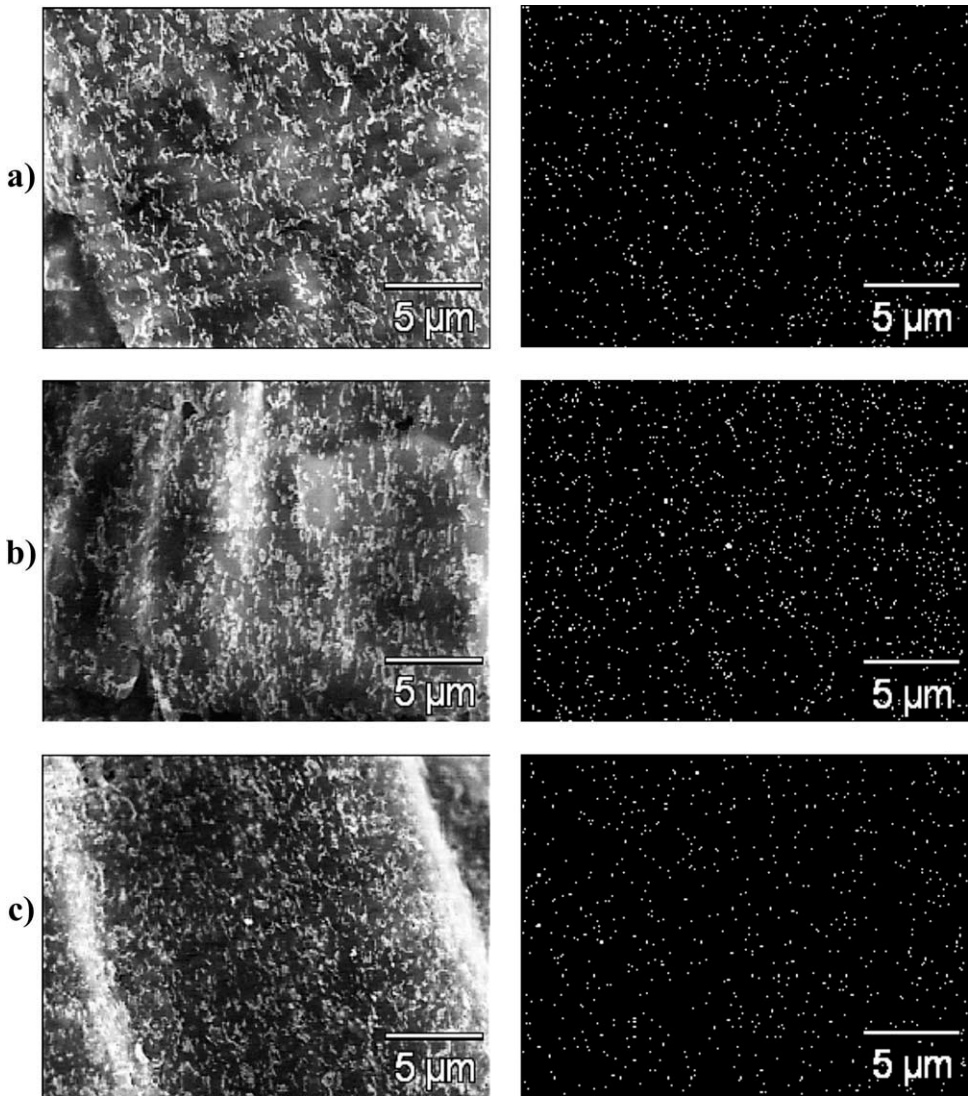

Figure 10. Micrographs of the extruded ABS/ZnO nanocomposites: (a) A-0.05, (b) A-0.17, and (c) A-3 (left: scanning electron, right: elemental mapping by EDX where white dots represent location of zinc element).

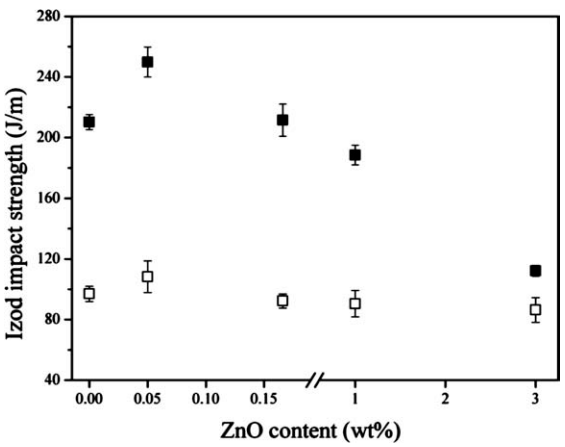

Figure 11. Izod impact strength as a function of ZnO content of ABS materials (□) before and (■) after extrusion process (error bar indicates standard deviation of up to 4 experiments).

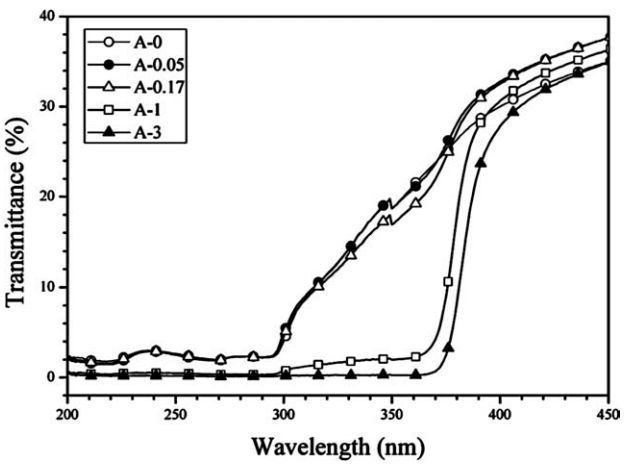

Figure 12. UV-Vis spectra of extruded ABS and ABS/ZnO nanocomposites.

macromolecular confinament and/or interacions between nanoparticles and SAN (matrix and/or grafts).

The UV protection increases as a function of ZnO content with a better performance in the nanocomposites obtained after extrusion as a consequence of nanoparticles agglomerates destruction.

ACKNOWLEDGMENTS

The authors thank María Luisa López, Jesús Ángel Cepeda, Myriam Lozano, Guadalupe Méndez, Jesús Rodríguez and Tonatiuh García for their support on issues related to electron microscopy, UV spectroscopy and polymer processing.

REFERENCES

1. Scheirsand, J.; Priddy, D. Modern Styrenic Polymers: Polystyrenes and Styrenic Copolymers, John Wiley and Sons Ltd., Chichester, UK, **2003.**
2. Adams, M. E., Buckley, D. J.; Colborn, R. E. *Rapra Rev. Rep.*, 6(10), report no. 70 (**1993).**
3. Kulich, D. M.; Gaggar, S. K.; Lowry, V.; Stepien, R. In Encyclopedia of Polymer Science and Technology; Mark, H. F., Ed.; John Wiley and Sons Inc., New York, USA, **2004.**
4. Cangelosi, F. A.; Davis, L. H.; Gray, R. L.; Stretanski, J. A.; Jakiela, D. J. In Encyclopedia of Polymer Science and Technology; Mark, H. F., Ed.;Wiley, **2004.**
5. Massey, L. K.; The Effects of UV Light and Weather on Plastics and Elastomers, William Andrew Publishing, Norwich, USA, **2007.**
6. Santos, R.; Botelho, G.; Machado. In Advanced Materials Forum V, Pt 1 and 2; Rosa, L. G.; Margarido, F., Eds.; Trans Tech Publications Ltd: Stafa-Zurich, **2010,** pp 772–778.
7. Ammala, A.; Hill, A. J.; Meakin, P.; Pas, S. J.; Turney, T. W. *J. Nanoparticle Res.* **2002,** *4*, 167.
8. He, J.; Shao, W.; Zhang, L.; Deng, C.; Li, C. J. *Appl. Polym. Sci.* **2009,** *114*, 1303.
9. Tang, E.; Cheng, G.; Pang, X.; Ma, X.; Xing, F. *Colloid Polym. Sci.* **2006,** *284*, 422.
10. Zhao, H. *Polymer* **2006,** *47*, 3207.
11. Chae, D. W.; Kim, B. C. *J. Appl. Polym. Sci.* **2006,** *99*, 1854.
12. Chae, D. W.; Kim, B. C. *Polym. Adv. Technol.* **2005,** *16*, 846.
13. Demir, M. M.; Castignolles, P.; Akbey, Ü.; Wegner, G. *Macromolecules,* **2007,** *40*, 4190.
14. Demir, M. M.; Memesa, M.; Castignolles, P.; Wegner, G. *Macromol. Rapid Commun.* **2006,** *27*, 763.
15. Zhao, G.; Guo, Q.; Yi, J.; Cai, X. J. *Appl. Polym. Sci.* **2011,** *122*, 2338.
16. Diaz de León, R.; Betancourt, R.; Puente, B. A.; Acuña, P.; Falcón, L. *Mater. Sci. Forum* **2010,** *644*, 135.
17. Kiamehr, M.; Moghaddam, F. M.; *Tetrahedron Lett.* **2009**, *50, 6723.*
18. Tsubokawa, N.; Kimoto, T.; Koyama, K. *Colloid Polym. Sci.* **1993,** *271*, 940.
19. Díaz de León, R.; Morales, G.; Acuña, P.; Soriano, F. *Polym. Eng. Sci.* **2010,** *50*, 373.
20. Chae, D. W.; Kim, B. C. *Macromol. Res.* **2010,** *18*, 772.
21. Chotirat, L.; Chaochanchaikul, K.; Sombatsompop, N.; *Intl. J. Adhesion Adhesives,* **2007,** *27*, 669.
22. Kim, I. J.; Kwon, O. S.; Park, J. B.; Joo, H. *Curr. Appl. Phys.* **2006,** *6 (Suppl. 1)*, e43.
23. Crosby, A. J.; Lee, J. Y. *Polym. Rev.* **2007,** *47*, 217.
24. Wang, X.; Wang, Z.; Wu, I. J. *Appl. Polym. Sci. 96*, 802.
25. Wang, Z.; Li, G.; Peng, H.; Zhang, Z.; Wang, X. J. *Mater. Sci.* **2005,** *40*, 6433.
26. Zhang, J.; Wang, X., Lu, L.; Li, D.; Yang, X. J. *Appl. Polym. Sci.* **2003,** *87*, 381.
27. Soriano, F.; Morales, G.; Díaz de León R. *Polym. Eng. Sci.* **2006,** *46*, 1698.
28. Choi, J. H.; Ahn, K. H.; Kim, S. Y. *Polymer* **2000,** *41*, 5229.